

## Nonlinear dynamics of a shell encapsulated microbubble near solid boundary in an ultrasonic field

N.M. Ali<sup>1,2</sup>, F. Dzaharudin<sup>1</sup> and E.A. Alias<sup>1</sup>

<sup>1</sup> Faculty of Mechanical and Automotive Engineering, Universiti Malaysia Pahang, 26600 Pekan, Pahang, Malaysia  
Phone: +6094246239; Fax: +609424222

**ABSTRACT** – Microbubbles have the potential to be used for diagnostic imaging and therapeutic delivery. However, the transition from microbubbles currently being used as ultrasound contrast agents to achieve its' potentials in the biomedical field requires more in depth understanding. Of particular importance is the influence of microbubble encapsulation of a microbubble near a vessel wall on the dynamical behaviour as it stabilizes the bubble. However, many bubble studies do not consider shell encapsulation in their studies. In this work, the dynamics of an encapsulated microbubble near a boundary was studied by numerically solving the governing equations for microbubble oscillation. In order to elucidate the effects of a boundary to the non-linear microbubble oscillation the separation distances between microbubble will be varied along with the acoustic driving. The complex nonlinear vibration response was studied in terms of bifurcation diagrams and the maximum radial expansion. It was found that the increase in distance between the boundary and the encapsulated bubble will increase the oscillation amplitude. When the value of pressure amplitude increased the single bubble is more likely to exhibit the chaotic behaviour and maximum radius also increase as the inter wall-bubble distance is gradually increased. While, with higher driving frequency the maximum radial expansion decreases and suppress the chaotic behaviour.

### ARTICLE HISTORY

Revised: 12<sup>th</sup> Feb 2020

Accepted: 04<sup>th</sup> Mar 2020

### KEYWORDS

*Dynamics;*  
*nonlinear;*  
*vibrations;*  
*ultrasound;*  
*microbubble;*  
*encapsulation;*  
*oscillation;*  
*boundary*

## INTRODUCTION

Microbubbles have been used as ultrasound contrast agents due to their ability to reflect the ultrasound waves in medical imaging hence empowering contrast [1-3]. These microbubbles have typical diameters in the range of 1-10  $\mu\text{m}$  allowing it to flow through microvessels and capillaries. This is due to significant difference in echogenicity between the gas in the microbubbles and the soft tissue surroundings of the body.

Recent studies have shown that microbubbles have the potential beyond contrasting agents. Microbubbles in conjunction with high intensity focused ultrasound transducer has great potential in the development of targeted imaging to characterize diseases at a molecular level in vivo [4, 5]. Furthermore, microbubbles also have the potential to be used in drug delivery, therapeutic agents, thrombolytic therapy [6], gene therapy, molecular imaging [7], anti-cancer therapy, and atherosclerotic therapy [4, 5]. One approach in drug delivery for example, is to incorporate drugs into microbubbles and selectively rupturing the bubbles to allow for local delivery into the feeder vessels of the lesion [4] thus increasing the efficacy of drug delivery. Though promising, many studies have shown particular interest with regards to if the agent has reached its' intended target at the vessel. This question is the motivation for this paper where we will attempt to identify how the vessel wall influence the microbubble oscillation.

It is interesting to note that most numerical work are based on the free gas bubble model i.e. bubbles that are not near any boundary, the Rayleigh model [8]. Over the years, the model was improved leading to other mathematical models governing microbubble oscillation such as the Rayleigh, Plesset, Noltingk, Neppiras, and Poritsky (RPNP) equation [9], Herring equation [10] and Keller-Miksis-Parlitz equation [11]. In recent years however, experimental studies have shown that the boundary have significant influence on microbubble oscillation. Garbin et al. [12] and Overvelde [13] for example have shown that the radial displacement can be higher in a bigger radius of vessels ( $\approx 100 \mu\text{m}$ ) compared to smaller radius vessels ( $\approx 10 \mu\text{m}$ ).

Furthermore, shell encapsulation of microbubble has also been shown to alter the acoustic properties and more stable than the free bubble gas [14]. Without encapsulation, microbubbles will dissolve spontaneously and nearly instantaneously due to the surface tension at the gas-liquid interface which is a problem for therapeutic applications. An encapsulating shell is necessary to sustain the gas cavity. Due to its' importance, there has been many studies over the years directed on modelling the shell encapsulation. For example, de Jong et al. [15-17] modelled the shell by taking into account elasticity and viscous friction of the encapsulating shell by modifying the Rayleigh-Plesset equation, Church et al. [18] assumed that the behaviour of shell material as viscoelastic and Morgan et al. [19] modified the Herring equation [10] to account for the viscosity, elasticity and the thickness of the encapsulating shell [19]. These studies, however, did not consider any boundary near the encapsulated bubbles. In this research, we try to extend the development of the dynamical behaviour of microbubble.

The objective of this paper is to investigate the effects of both; the boundary and the encapsulating shell, on the nonlinear microbubble response in an ultrasonic field will be studied which are closer to the scenario in clinical studies.

## METHODS AND MATERIALS

In this section the mathematical modelling of the free gas bubble will be modified to include the effect of shell and encapsulation and boundary. The type of shell that will be used in this paper is a commercial microbubble, MP1950 (Mallinckrodt, Inc., St. Louis, MO). It is a phospholipid type of shell and a decafluorobutane core commonly used for streak microscopy [19, 20] .

Here we would like to investigate how the acoustic parameters and interbubble-wall distance influence the transition from periodic to chaotic oscillation. Since nonlinear oscillations are notorious for the significant changes in the overall dynamics given a small parameter change, we shall limit the study to a manageable set of parameters as outlined below to achieve the objective of this study:

*Effects of ultrasound acoustic driving frequency:* The bifurcation diagrams in Figure 4 were obtained with respect to ultrasound acoustic driving frequency,  $f_{ext}$  , as the control parameter and acoustic driving pressure,  $\alpha = 150$  kPa, as the constant parameter.

*Effects of ultrasound acoustic driving pressure:* The bifurcation diagrams in Figure 5 were obtained with respect to ultrasound acoustic driving pressure,  $\alpha$ , as the control parameter and driving frequency,  $f_{ext} = 1.5$  MHz, as constant pressure.

*Effects of distances between boundary and encapsulated microbubble:* The bifurcation diagrams labelled (a)-(d) in Figures 4-6 were plotted by varying separation distance between the bubble and boundary,  $d/R_0 = 2.5, 5, 10$  and  $15$  respectively.

### Mathematical Modelling

To model an encapsulated bubble near a boundary as shown in Figure 1, we first consider a free bubble model, the Keller-Miksis-Parlitz (KMP) equation which has the advantage over other models as it is suitable for large radial oscillations. The KMP equation is given by

$$\left[ 1 - \left( \frac{\dot{R}}{c} \right) \right] R \ddot{R} + \frac{3}{2} \left[ \frac{\dot{R}}{3c} \right] \dot{R}^2 = \frac{1}{\rho} \left[ \left( \frac{\dot{R}}{c} \right) + \left( \frac{R}{c} \frac{d}{dt} \right) \right] \left[ P(R, \dot{R}) - P_{\infty}(t) \right] \tag{1}$$

The variables and their associated parameter values are shown in Eq. (1) at 20°C. is given in Table 1. Here,  $P_{\infty}(t) = P_0 - P_v + \alpha \sin(\omega t)$ , represents the pressure in the liquid far from the bubble where  $\omega$  is the angular frequency,  $\omega = 2\pi f_{ext}$ ,  $\alpha$  is the acoustic pressure amplitude and  $f_{ext}$  is the acoustic frequency. The initial conditions  $R(0) = R_0$  and  $dR/dt(0)=0$  were imposed indicating that at time  $t=0$ , the bubble has an initial radius of  $R_0$  and is motionless.

**Table 1.** Parameters for the bubble model

Symbol	Description	Value
$R_0$	Intial bubble radius	2.0 $\mu\text{m}$
$\mu$	Dynamic viscosity of the liquid	0.001 kg/m s
$\rho$	Density of the liquid	998.2 kg/cm <sup>3</sup>
$\kappa$	Polytropic exponent for the gas bubble	1.07
$c$	Speed of sound in air	1484 m/s
$\sigma$	Surface tension of the bubble surface	0.051 N/m
$P_v$	Hydrostatic pressure outside bubble	2330 Pa
$P_0$	Pressure inside the bubble	100,000 Pa

$$P(R, \dot{R}) = \left( P_0 - P_v + \frac{2\sigma}{R_0} + \frac{2\chi}{R_0} \right) \left( \frac{R_0}{R} \right)^{3\kappa} - \frac{4\mu\dot{R}}{R} - \frac{2\sigma}{R} - \frac{2\chi}{R} \left( \frac{R_0}{R} \right)^2 - 12\varepsilon\mu_{sh} \frac{\dot{R}}{R(R-\varepsilon)} \tag{2}$$

The model assumes that the bubble will remain spherical throughout the oscillation. In this study, we will limit our scope to the parameter space in which the microbubble does not undergo collapse and remain spherical in shape. To incorporate the encapsulating shell of thickness  $\varepsilon$  as shown in Figure 1, the  $P(R,R)$  term in Eq. (1) will be modified following Morgan et al. [19]. where  $\chi$  is the shell elasticity, and  $\mu_{sh}$  is the shell viscosity. Here, a commercially produced microbubble MP1950 will be used with the parameter values of  $\varepsilon = 1$  nm,  $\mu_{sh} = 1$  Pa.s and  $\chi = 0.5$  N/m [19].

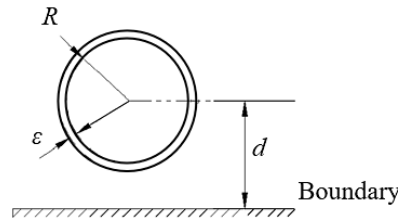


**Figure 1.** Schematic diagram of a single shell encapsulated bubble near solid boundary where  $d$  is the distance between the centre of the bubble with the boundary

Up to this point, the equation we have derived is for a microbubble with a shell encapsulation in infinite medium. In order to include the effects of a wall as shown in Figure 1, the mirror image methods will be used following the derivation by Dzaharudin et al. [21] where the following term will be incorporated in Eq. (1),

$$P_w = -\frac{1}{2d} \left( R^2 \ddot{R} + 2R\dot{R}^2 \right) \tag{3}$$

Here  $d$  is the distance between the wall and the bubble centre (see Figure 1). In this paper, the interbubble-wall distance will be varied as follows;  $d/R_0 = 2.5, 5, 10$  and  $15$ . Thus, the governing equation of an encapsulated microbubble near a boundary is given by,

$$\left[ 1 - \left( \frac{\dot{R}}{c} \right) \right] R\ddot{R} + \frac{3}{2} \left[ \frac{\dot{R}}{3c} \right] \dot{R}^2 = \frac{1}{\rho} \left[ \left( \frac{\dot{R}}{c} \right) + \left( \frac{R}{c} \frac{d}{dt} \right) \right] \left[ P(R, \dot{R}) - P_\infty(t) \right] - P_w \tag{4}$$

where,  $P(R,R)$  is given by Eq. (2) and  $P_w$  is given by Eq. (3). To ensure the validity of Eq. (3), the simulations will be stopped as soon as the bubble wall collides with the boundary. A typical solution of the ordinary differential equation in Eq. (4) will result in a time series as shown in Figure 2.

### Validation

In this section, we will compare the results of our code with those in published literature Li et al. [22] where they study the effect of a solid boundary on the dynamics of a small group of ultrasound driven microbubbles. This method is to ensure the validity of the numerical solving code.

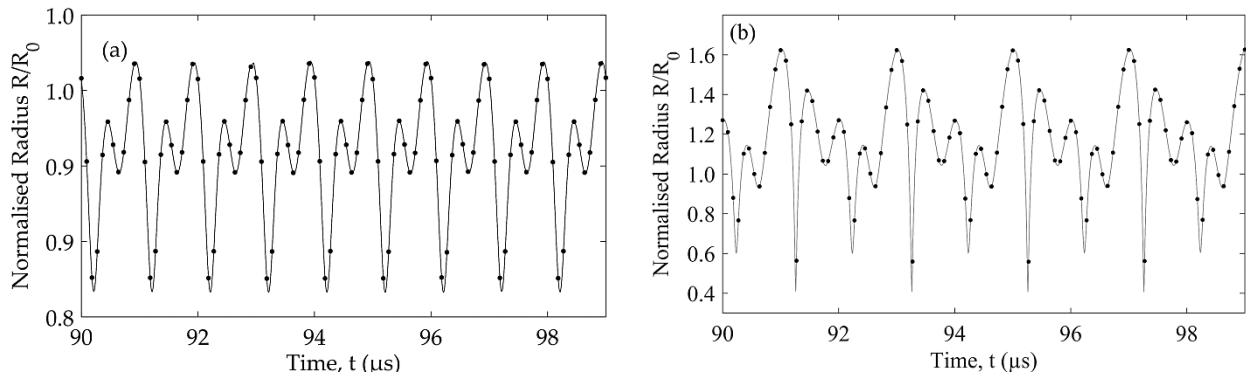


**Figure 2.** Comparison between results obtained from code (line) with Figure 5 from Li et al. [22] (black dots) for a microbubble with size  $R_0 = 2.0 \mu\text{m}$  positioned  $d/R_0 = 15$  away from a solid wall subjected to an ultrasonic frequency of 1 MHz and driving pressure of (a) 40 kPa and (b) 125 kPa

We extract our result using in MATLAB ® ODE 15s as numerical solver. Figure 2 shows the comparison between the output of our code (represented by the solid line) and that from Figure 5 in the paper published by Li et al. [22] studied the (represented by the black dots). We set the parameter same as the as in the paper published by Li et al. [22] where a single bubble with initial radius  $R_0 = 2.0 \mu\text{m}$  located  $d/R_0 = 15$  from the wall was subjected to an ultrasound pressure amplitude of 40 kPa and 125 kPa.

The plot good agreement between our output and with published results since the black dots fall exactly on the solid line as seen in Figure 2(a) and (b). This validation method has been use by several researchers [21].

## RESULTS

The dynamical response of a microbubble subjected to ultrasound is a complex nonlinear problem which belongs to a class of driven nonlinear oscillators. This class are deterministically chaotic systems with all their involved and complex dynamics. In order to study these types of oscillators, we shall employ a method from chaos theory to visualise the parameter dependence of the dynamics of the bubble via bifurcation diagrams. In theory, the driven bubble oscillation may be periodic and chaotic.

Left column in Figure 3 shows the typical the radius-time after transients have decayed obtained numerically solving Eq. (4) for a  $R_0 = 2 \mu\text{m}$  MP1950 microbubble located at  $d/R_0 = 15$  from the boundary subjected to a driving frequency of 1 MHz. The right column is the phase space diagram representation of the radius-time response. The top to the bottom rows of Figure 3 corresponds to increasing pressure amplitude: 40 kPa, 125 kPa and 250 kPa. The dots represent points at the end of each acoustic cycle,  $T = 1/f_{ext}$ . Note that the axes range in Figure 3 are not the same and are chosen to clearly illustrate the outline of the trajectories.

In Figure 3(a) and (c) the normalised radius,  $R/R_0$ , at the end of each driving period,  $T$ , is the same; effectively repeating itself after every time interval length of  $T$  but with different maximum normalised radius. As for 40 and 125 kPa, the maximum normalised radius is  $R/R_0 = 1.12$  and  $R/R_0 = 1.5$  respectively. These corresponds to a single period oscillation which is represented as one dot on the phase diagram in Figure 3 (b) and (d), where  $V = dR/dt$  is the bubble wall velocity. The phase diagram reveals a crossing trajectory with on dot as the bubble returns to its original state within a single period of driving,  $T$ . With increased driving pressure at 250 kPa, as shown in Figure 3(e), the dots no longer repeated itself after multiples of  $T$  and resulting to chaos phase. This observation corresponds to the spread of dots seen in the phase space diagram in Figure 3(f).

Figure 4 below shows pressure bifurcation used in clinical studies [23] for a  $R_0 = 2 \mu\text{m}$  MP1950 encapsulated microbubble subjected to  $f_{ext} = 1 \text{ MHz}$  for varying inter bubble-wall distances for Figures 4(a)  $d/R_0 = 2.5$ , 4(b)  $d/R_0 = 5$ , 4(c)  $d/R_0 = 10$  and 4(d)  $d/R_0 = 15$ .

The normalised radial response and phase diagram in Fig. 3 are represented as a bifurcation diagram in Fig. 4(d), where the coordinate value of the point in the phase space is plotted versus a parameter of the model, called control parameter. In Figure 4 the control parameter is the driving pressure amplitude,  $\alpha$  as the constant parameter is the driving frequency,  $f_{ext} = 1 \text{ MHz}$ .

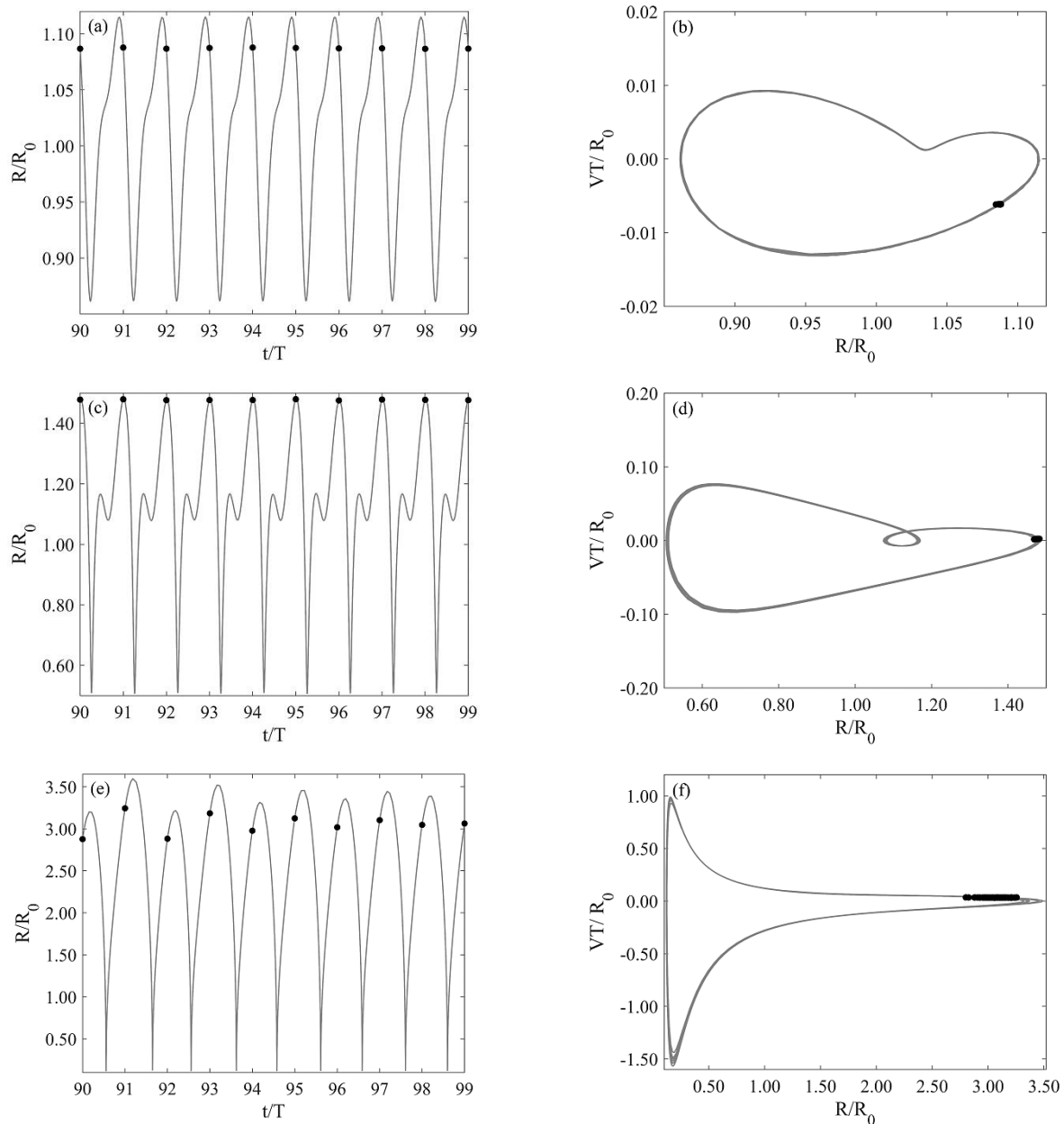


**Figure 3.** Left column shows the normalised radial response of a  $R_0 = 2 \mu\text{m}$  gas bubble located at  $d/R_0 = 15$  from the boundary and insolated by a sinusoidal pressure wave of frequency,  $f_{ext} = 1 \text{ MHz}$ . The driving pressure amplitude increases from top to bottom as 40 kPa, 125 kPa and 250 kPa. The right-hand column shows the phase space diagram representation of the radius-time response. Black dots represent points at the end of each acoustic cycle,  $T = 1/f_{ext}$

In Figure 4(d), the single period-1 solution obtained from the phase diagram for  $\alpha = 40$  (Figure 3(b)) and 125 kPa (Figure 3(d)) yields one point at the value of the control parameter,  $\alpha = 40$  and 125 kPa in Figure 4(d). Phase diagram in Figure 3(f) show a chaotic response, the projection of dots from the phase diagram on the bifurcation diagram in Figure 4(d) corresponds to the large number of points spread along the vertical line at  $\alpha = 250$  kPa. This is where the system changes between order and chaotic signifying that an alter in control parameter can make a steady system in chaos. The distance between bubble and wall,  $d/R_0 = 2$  in Figure 4(a) show a single period-1 solution obtained from the phase diagram in Figure 4(b) for  $\alpha < 120$  kPa. And it stops as the bubble hit the wall afterwards.

The structure in Figure 4(b) appear that the shell encapsulated bubble showing more chaotic dynamic behaviour for higher amplitude pressure. Where, the bubble undergoes a single period oscillation right before experiencing a period doubling bifurcation at  $\alpha = 200$  kPa, after the bubble exhibits a ‘jump’ similar to researcher Li et. al. [22] (refer Figure 6) at the onset of chaos at  $\alpha = 150$  kPa. This is a characteristic of a saddle node bifurcation, followed by a series of period-doubling bifurcations that leads to chaotic behaviour. A chaotic response signifies a highly nonlinear dynamic behaviour that could increase drug/gene intake by applying shear stress on cell membranes [24, 25].

Upon considering the effects of boundary proximity, the chaotic oscillations diminish (see Figures. 4(b) - (d)) as the distance of boundary is increase and more periodic oscillations are observed. Based on these observations bubble oscillate

and tends to enter the route to chaos as the amplitude pressure is increase when the system subjected to a driving ultrasound frequency,  $f_{ext} = 1$  MHz. It is also observed that the microbubble system undergo chaotic oscillations at higher pressure amplitude as the distance between the bubble and the solid boundary is decreased.

The control parameter is the driving pressure amplitude with frequency bifurcation diagrams were computed in Figure 5 to allow us to analyse the effect of varying the ultrasound frequency to dynamical behaviour encapsulated microbubble near boundary proximity. The ultrasound frequency,  $f_{ext}$ , was taken as the control parameter and the bubble was driven at  $\alpha = 150$  kPa in Figure 5. Each bifurcation diagram is plotted with the varying inter bubble-wall distances from Figure 5(a)  $d/R_0 = 2.5$ , Figure 5(b)  $d/R_0 = 5$ , Figure 5(c)  $d/R_0 = 10$ , and Figure 5(d)  $d/R_0 = 15$ .

In Figure 5(a) the computations was stopped for  $f_{ext} < 1.15$  MHz since the bubble wall collides with the solid boundary. The response of the shell encapsulated bubble generally contains of single period and double period oscillations throughout the control parameter range, where it starts with period 2 at  $f_{ext} \sim 1.15$  MHz and transitions to period 1 oscillation at  $f_{ext} \sim 1.17$  MHz. As the bubble moves further away from the boundary (compare Figures. 5(a)-(d)), the chaos region shrink. In Figure 5(b)-(d) the increase in frequency of the ultrasound driving results in two saddle node bifurcations characterised by the sudden “jumps” meanwhile at inter bubble-wall distance,  $d/R_0 = 2.5$  the absence of “jumps” same as published paper of MacDonald et. al [26] (refer Figure 3).

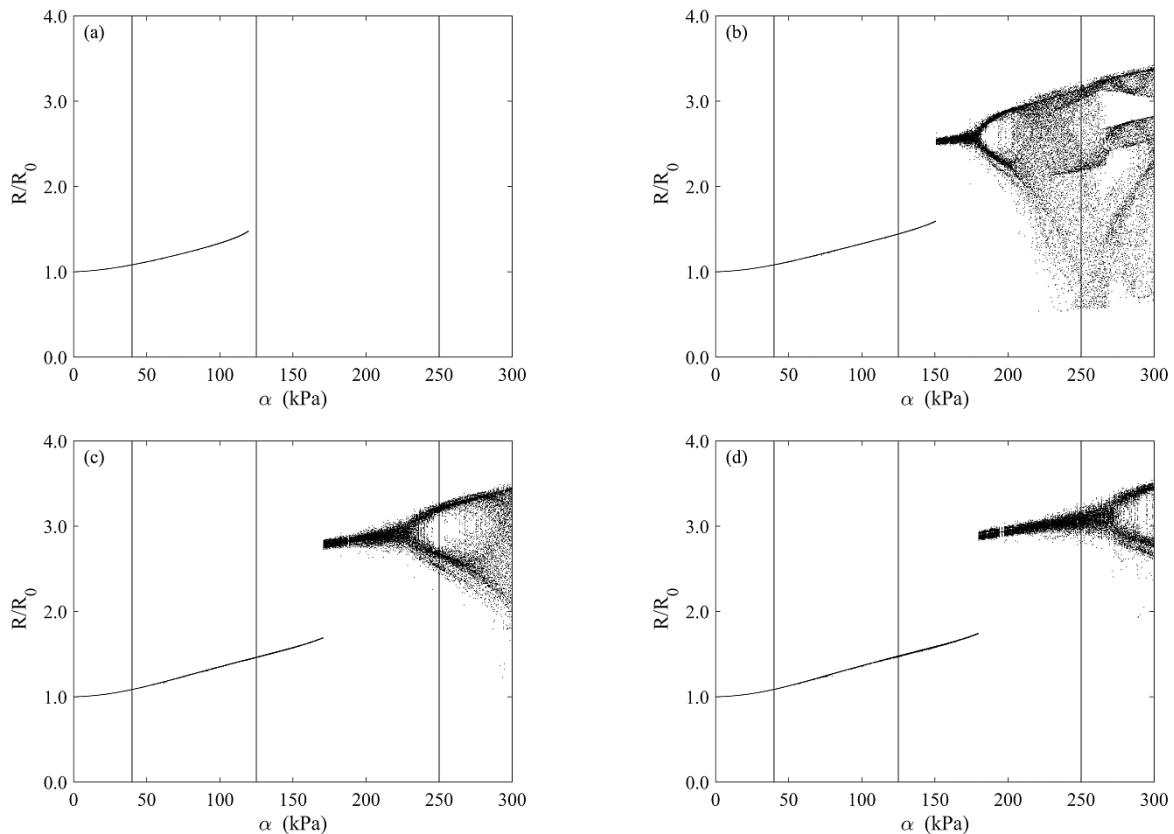


**Figure 4.** Bifurcation characteristics showing the normalised radius versus the acoustic driving pressure,  $\alpha$ , for  $f_{ext} = 1$  MHz for (a)  $d/R_0 = 2.5$ , (b)  $d/R_0 = 5$ , (c)  $d/R_0 = 10$  and (d)  $d/R_0 = 15$ . The initial size of the microbubble is  $R_0 = 2 \mu\text{m}$ . The three vertical lines in the figure shows reference location where  $\alpha = 40, 125$  and  $250$  kPa

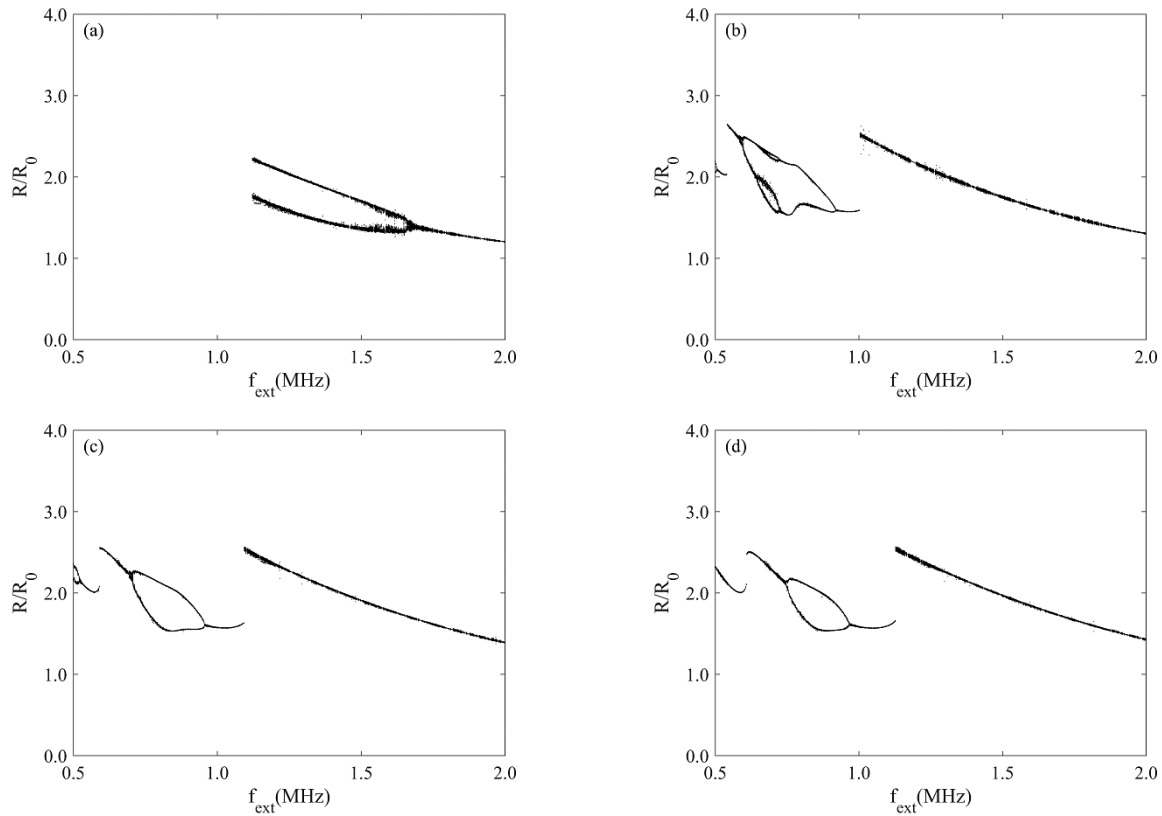


**Figure 5.** Bifurcation characteristics showing the normalised radius versus the driving frequency for  $\alpha = 150 \text{ kPa}$  for (a)  $d/R_0 = 2.5$ , (b)  $d/R_0 = 5$ , (c)  $d/R_0 = 10$ , (d)  $d/R_0 = 15$ . The initial size of the microbubble is  $R_0 = 2 \mu\text{m}$

### Maximum Radius

In the previous section, the bifurcation diagrams of pressure amplitude and driving frequency as control parameter computed only provides information of the frequency content of the bubble behaviour.

Here, the maximum radial expansion ratio of the encapsulated gas bubble changes as the driving pressure amplitude (Figure 6(a)) and driving frequency (Figure 6(b)) increases will be studied. The maximum radial expansion of the encapsulated microbubble,  $R_{max}$  provides a significant understanding in how changing the boundary proximity combined with varying control parameters whether is the driving frequency or acoustic pressure amplitude. There are numerous of applications such as local drug delivery and gene therapy, require identification of parameters that will contribute to large bubble oscillations leading to bubble rupture and collapse. Some applications such as drugs transportation with a targeted site inside the body, the practice requires a significant identification of physical parameters that eventually give rise to large microbubble oscillation [21, 27]. There is study suggested that the possibility of bubble collapse hence releasing localised drug, is higher for larger values of maximum radius [21, 28].

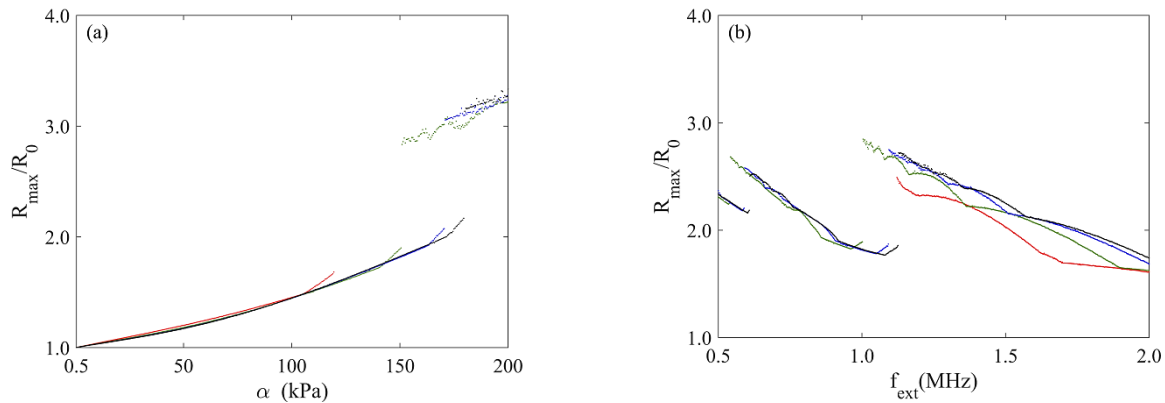


**Figure 6.** Maximum radial expansion,  $R_{max}$  for a microbubble with an initial radius  $R_0 = 2 \mu\text{m}$  subjected to (left) constant ultrasound pressure amplitude and (right) constant ultrasound frequency for (a)  $f_{ext} = 1 \text{ MHz}$  (b)  $\alpha = 150 \text{ kPa}$ . The colours represent the boundary proximity for the bubble-boundary separation distance  $d/R_0 = 2.5$  (red),  $d/R_0 = 5$  (green),  $d/R_0 = 10$  (blue),  $d/R_0 = 15$  (black)

The computation of bubble response for all points of bifurcation in Figures. 4 and 5 the maximum radius,  $R_{max}$  was also have been obtained for increasing proximity to the boundary, distance  $d/R_0 = 2.5$  (red),  $d/R_0 = 5$  (green),  $d/R_0 = 10$  (blue),  $d/R_0 = 15$  (black). It appears a clear trend on how  $R_{max}$ , changes with boundary proximity. From Figure 6(a) and (b) that as the microbubble is moved closer to the solid boundary tends to decrease  $R_{max}$ . In Fig. 6, there is a consistent observation that the sudden “jumps” in the value of  $R_{max}$  is followed by a more gradual increase of  $R_{max}$ . With a further study, each time there is a saddle node bifurcation in the corresponding Figures 4 and 5 the “jumps” will occur. This show there is connection with the fundamental frequency and their harmonics as this type of bifurcation occurred [11]. The sudden expansion in maximum radial of oscillation may lead to forceful rupture due to the increase in inertial forces. This occurrence has been proven to be useful in local drugs release and gene release into microvessel walls and cell membrane [29, 30].

## CONCLUSIONS

Microbubbles have been shown to have the potential to redraw the boundaries of therapeutic and theranostic applications. However, the influence of shell encapsulation of a microbubble near a wall vessel remains unclear. Shell encapsulation is important in therapeutic applications as it stabilizes the bubble. However, many bubble studies investigate gas bubbles without a shell. Furthermore, most studies do not consider the boundary effects which is important in medical applications. To solve this, we modified a Keller-Miksis-Parlitz model that included the encapsulating shell and boundary effects. It was found that the combined influence of boundary proximity and shell encapsulation may cause a shift in the fundamental frequency of the bubbles by observing the effect distances between boundary and encapsulated microbubble and the changes of maximum radial expansion by varying the driving frequency or acoustic pressure. Moreover, it shows that the encapsulated bubble dynamic oscillations were suppressed with increasing separation distance between the bubble and boundary due to the presence of more periodic oscillations instead of broadband response. Also, the effect of ultrasonic acoustic driving pressure gives a significant finding where the higher the amplitude pressure apply to microbubble the higher chance for the bubble to collapse as show in maximum radial expansion. In addition, the expansion of maximum radial decreased when the driving frequency higher and more likely stable as shown in bifurcation diagram.

## ACKNOWLEDGMENTS

The authors would like to acknowledge Malaysia Ministry of Education (FRGS/1/2017/TK03/UMP/03/1) and Universiti Malaysia Pahang, Malaysia (RDU160398 and PGRS190333).

## REFERENCES

- [1] A. L. Klibanov, "Microbubble Contrast Agents: Targeted Ultrasound Imaging and Ultrasound-Assisted Drug-Delivery Applications," *Investigative Radiology*, vol. 41, pp. 354-362, 2006.
- [2] P. J. Frinking, A. Bouakaz, J. Kirkhorn, F. J. Ten Cate, and N. de Jong, "Ultrasound contrast imaging: current and new potential methods," *Ultrasound in Medicine & Biology*, vol. 26, pp. 965-975, 2000.
- [3] R. Gramiak and P. M. Shah, "Echocardiography of the aortic root," *Investigative Radiology*, vol. 3, pp. 356-366, 1968.
- [4] K. W. Ferrara, "Driving delivery vehicles with ultrasound," *Advanced Drug Delivery Reviews*, vol. 60, pp. 1097-1102, 2008.
- [5] K. W. Ferrara, R. Pollard, and M. Borden, "Ultrasound microbubble contrast agents: fundamentals and application to gene and drug delivery," *Annual Review of Biomedical Engineering*, vol. 9, 2007.
- [6] A. L. Klibanov, "Targeted delivery of gas-filled microspheres, contrast agents for ultrasound imaging," *Advanced Drug Delivery Reviews*, vol. 37, pp. 139-157, 4/5/ 1999.
- [7] S. Wang, J. A. Hossack, and A. L. Klibanov, "Targeting of microbubbles: contrast agents for ultrasound molecular imaging," *Journal of drug targeting*, vol. 26, pp. 420-434, 2018.
- [8] L. Rayleigh, "VIII. On the pressure developed in a liquid during the collapse of a spherical cavity," *The London, Edinburgh, and Dublin Philosophical Magazine and Journal of Science*, vol. 34, pp. 94-98, 1917.
- [9] B. C. Eatock, R. Y. Nishi, and G. W. Johnston, "Numerical studies of the spectrum of low-intensity ultrasound scattered by bubbles," *The Journal of the Acoustical Society of America*, vol. 77, pp. 1692-1701, 1985.
- [10] C. Herring, *Theory of the pulsations of the gas bubble produced by an underwater explosion*: Columbia Univ., Division of National Defense Research, 1941.
- [11] U. Parlitz, V. Englisch, C. Scheffczyk, and W. Lauterborn, "Bifurcation structure of bubble oscillators," *The Journal of the Acoustical Society of America*, vol. 88, pp. 1061-1077, 1990.
- [12] V. Garbin, D. Cojoc, E. Ferrari, E. Di Fabrizio, M. Overvelde, S. Van Der Meer, *et al.*, "Changes in microbubble dynamics near a boundary revealed by combined optical micromanipulation and high-speed imaging," *Applied Physics Letters*, vol. 90, p. 114103, 2007.
- [13] M. Overvelde, V. Garbin, J. Sijl, B. Dollet, N. De Jong, D. Lohse, *et al.*, "Nonlinear shell behavior of phospholipid-coated microbubbles," *Ultrasound in medicine and biology*, vol. 36, pp. 2080-2092, 2010.

- [14] L. Hoff, P. C. Sontum, and J. M. Hovem, "Oscillations of polymeric microbubbles: Effect of the encapsulating shell," *The Journal of the Acoustical Society of America*, vol. 107, pp. 2272-2280, 2000.
- [15] N. de Jong, R. Cornet, and C. Lancee, "Higher harmonics of vibrating gas-filled microspheres. Part one: simulations," *Ultrasonics*, vol. 32, pp. 447-453, 1994.
- [16] N. de Jong and L. Hoff, "Ultrasound scattering of Alunex® microspheres Ultrasonics," *Ultrasonics*, vol. vol. 31, pp. 175-181, 1993.
- [17] N. de Jong, L. Hoff, T. Skotland, and N. Bom, "Absorption and scatter of encapsulated gas filled microspheres: theoretical considerations and some measurements," *Ultrasonics*, vol. 30, pp. 95-103, 1992.
- [18] C. C. Church, "The effects of an elastic solid surface layer on the radial pulsations of gas bubbles," *The Journal of the Acoustical Society of America*, vol. 97, pp. 1510-1521, 1995.
- [19] K. E. Morgan, J. S. Allen, P. A. Dayton, J. E. Chomas, A. Klibaov, and K. W. Ferrara, "Experimental and theoretical evaluation of microbubble behavior: effect of transmitted phase and bubble size," *IEEE Transactions on Ultrasonics, Ferroelectrics, and Frequency Control*, vol. 47, pp. 1494-1509, 2000.
- [20] B. Helfield, "A Review of Phospholipid Encapsulated Ultrasound Contrast Agent Microbubble Physics?," *Ultrasound in medicine & biology*, 2018.
- [21] F. Dzaharudin, A. Ooi, and R. Manasseh, "Effects of boundary proximity on monodispersed microbubbles in ultrasonic fields," *Journal of Sound and Vibration*, vol. 410, pp. 330-343, 2017.
- [22] M. Li, F. Dzaharudin, A. Ooi, and R. Manasseh, "The effect of a solid boundary on the dynamics of a small group of ultrasound driven microbubbles," in *Proceedings of the 20th International Congress on Acoustics*, 2010, pp. 639-646.
- [23] A. N. Pouliopoulos and J. J. Choi, "Superharmonic microbubble Doppler effect in ultrasound therapy," *Physics in Medicine and Biology*, vol. 61, pp. 6154-6171, 2016/07/29 2016.
- [24] I. Lentacker, S. C. De Smedt, and N. N. Sanders, "Drug loaded microbubble design for ultrasound triggered delivery," *Soft Matter*, vol. 5, pp. 2161-2170, 2009.
- [25] D. H. Edwards, Y. Li, and T. M. Griffith, "Hydrogen peroxide potentiates the EDHF phenomenon by promoting endothelial Ca<sup>2+</sup> mobilization," *Arterioscler Thromb Vasc Biol.*, vol. 28, pp. 1774-1781, 2008.
- [26] C. Macdonald and J. Gomatam, "Chaotic dynamics of microbubbles in ultrasonic fields," *Proceedings of the Institution of Mechanical Engineers, Part C: Journal of Mechanical Engineering Science*, vol. 220, pp. 333-343, 2006.
- [27] I. Lentacker, S. C. De Smedt, and N. N. Sanders, "Drug loaded microbubble design for ultrasound triggered delivery," *Soft Matter*, vol. 5, pp. 2161-2170, 2009.
- [28] C. E. Brennen, "Fission of collapsing cavitation bubbles," *Journal of Fluid Mechanics*, vol. 472, pp. 153-166, 2002.
- [29] M. A. Rajendran, "Ultrasound-guided Microbubble in the Treatment of Cancer: A Mini Narrative Review," *Cureus*, vol. 10, pp. 1-4, 2018.
- [30] T.-Y. Wang, K. E. Wilson, S. Machtaler, and J. K. Willmann, "Ultrasound and Microbubble Guided Drug Delivery: Mechanistic Understanding and Clinical Implications," *Curr Pharm Biotechnol*, vol. 14, pp. 743-752, 2014.